Polymer Bulletin
https://doi.org/10.1007/s00289-020-03278-1

ORIGINAL PAPER

Electrochemical characteristics of solid state double-layer capacitor constructed from proton conducting chitosan-based polymer blend electrolytes

Shujahadeen B. Aziz[1,2] · M. A. Brza[1,3] · H. M. Hamsan[4] · M. F. Z. Kadir[4] · Rebar T. Abdulwahid[1,5]

Received: 18 January 2020 / Revised: 6 May 2020 / Accepted: 13 June 2020

Abstract

This research is about the preparation of polymer blend electrolytes based on chitosan using solution cast technique. Field emission scanning electron microscopy and Fourier transform infrared spectroscopy (FTIR) routes were utilized for studying morphological and structural properties, respectively. Electrical impedance spectroscopy (EIS) was engaged for determining the direct current electrical conductivity of the films. The ion association at the highest salt concentration was actually present as confirmed by EIS and FTIR achievements. The sample surface displays the protrude salts at the highest salt concentration. Proton conducting polymer electrolyte with NH_4Br as H^+ (proton) provider has been used in electric double-layer capacitor (EDLC) applications. The highest conducting sample was used to fabricate EDLC. The transference number measurement indicated that the sample is mostly includes ion charge carriers which are vital for application in electrochemical devices. The linear sweep voltammetry study revealed that the decomposition of the sample takes place above 1.54 V. The fabricated EDLC device was performed capacitive behavior, as it can be seen from the cyclic voltammetry (CV) plot. Since no redox peaks have appeared, it can be concluded that the EDLC did not undergo either oxidation or reduction. The acquired value of specific capacitance (132.5 Fg^{-1}) is considered to be of great interest from the application viewpoints.

Keywords Polymer blends electrolytes · FTIR study · Electrical impedance spectroscopy · TNM and LSV analysis · CV · EDLC device

✉ Shujahadeen B. Aziz
shujaadeen78@yahoo.com; shujahadeenaziz@gmail.com

Extended author information available on the last page of the article

Published online: 18 June 2020

Introduction

Using natural biopolymers instead of the synthetic polymers may solve plastic waste pollution [1, 2]. Accordingly, researchers will be more strained their attention toward the preparation of polymer electrolytes based on natural polymers. Safety, portability, low-cost, great flexibility, good thermal stability, and light weight are some of the interesting features of SPEs [3]. Dextran (Dex) is a natural biopolymer and it is broadly used in the medicine industry as drug carriers. There are 1,6-α-D-glucopyranosidic linkages in dextran's structure [4]. There are many oxygen functional groups on the backbone of dextran chains which is crucial for salt dissociation. With such properties, a polymer electrolyte can be made out of it [5]. As suggested by Hamsan et al. [6], there is a system of Dex-ammonium nitrate (NH_4NO_3) that has a maximum DC conductivity of 10^{-5} S/cm. On the other hand, chitosan (CS) is biodegradable and non-toxic and possesses good film-producing characteristics; and thus it is very popular for the polymer blend system. Crabs, prawns and other skeletons from the ocean are sources for CS manufacture [7]. In addition, crustaceans having β-(1 → 4)2-amino-2-deoxy-D-glucose-(D-glucosamine) structure can also produce CS [7]. It is well-reported that the properties of single polymer can be enriched through polymer bending methodology. A carbon-based blended polymer and polymer nanocomposites have shown many favorable properties for energy storage device applications [8–10]. The polymer film gets enhanced mechanical strength by collectively blending various structures of miscible polymers [11]. One type of electrochemical capacitor is electrical double-layer capacitor (EDLC) in which the energy storage mechanism based on the accumulation of charge at the surface of carbon electrode and it turns into potential energy [12]. Rapid charge–discharge rate, straightforward fabrication technique, great power density, and long cycle life are some of the desired features of EDLC device [13]. There has been utilization of graphite [14], aerogel [15], carbon nanofiber [16], activated carbon [17], and other active materials as electrode of EDLC. Since activated carbon has affordability, high surface area, and good electronic conductivity, it is a good candidate as an active material for electrodes of EDLC [18]. Regular batteries can be replaced with EDLC. However, there is a need for further investigation on how charge storage works in EDLC. Both industrial and fundamental elements can benefit from the study of energy storage mechanism in microporous materials. Moving forward, researchers will be able to make this technology more widespread in the industry because more robust supercapacitors can be designed more easily. Non-Faradaic reaction at the electrode/electrolyte interface results in the formation of a double-layer of ions [19]. Furthermore, affordability, greater reversibility, enhanced thermal stability, and simplicity in fabrication are benefits of EDLC device compared to pseudocapacitor or Faradaic capacitors [20–22]. Nevertheless, Eftekhari [23] showed that energy storage system can also work by accommodating ions within mesoporous and microporous instead forming a double-layer capacitor. Henceforth, the classical model (wherein energy storage devices undergo charge separation and storage via ions) has some dissimilarity

with the mentioned mechanism. With that being said, the electrode surface gains the charged species devoid of chemical interactions since the inner layer (created by the electrostatic forces) powers the classical models. Taking into consideration, it should be perfectly possible to polarize the double-layer charging on the surface of the electrode [24].

Strong inorganic acids or ammonium salts are normally used in the preparation of proton (H^+) conducting solid polymer electrolytes (SPEs). Phosphoric acid (H_3PO_4) and sulfuric acid (H_2SO_4) are some of the inorganic acids utilized. Nonetheless, SPEs having inorganic acids face chemical degradation and thus, are out of actual use [25, 26]. Thus, a proton conducting SPE having high thermal stability and ionic conductivity be able to be achieved using ammonium salts. The lattice energy of ammonium chloride (NH_4Cl) is 698 kJ/mol, while that of ammonium bromide (NH_4Br) is 665.3 kJ/mol [27]. Ionic dissociation will be simpler since the lattice energy is low [28]. According to our prior researches [29, 30], using 40 wt% Dex to blend 60 wt% CS yields minimum crystallinity. Hence, 60 wt% CS–40 wt% Dex blend has been incorporated with NH_4Br in different concentrations in the current work. By comparing the findings of this research to those in the literature, electrochemical devices can be fabricated by considering the salts' lattice energy. EDLC will be fabricated in the current work by using the electrolyte with highest DC conductivity.

Materials and methods

Sample preparation

The raw materials were chosen to be Dextran (Dex) powder (average molecular weight 35,000–45,000) and high molecular weight chitosan (CS) (average molecular weight 310,000–375,000) materials (Sigma-Aldrich). To fabricate the CS:Dex-based polymer blending, 60 mL of 1% acetic acid was used to individually dissolve 40 wt% Dex and 60 wt% CS at ambient temperature for 1.5 h. Afterward, a homogeneous blending solution was achieved by mixing and stirring these solutions for 180 min. For the preparation of CS:Dex:NH_4Br electrolytes, the blended solution of CS:Dex incorporated with various amounts of NH_4Br ranging from 10 to 40 wt% with the difference of 10 wt% while being constantly stirred. The polymer blend electrolytes were coded as CSDXN0, CSDXN1, CSDXN2, CSDXN3, and CSDXN4 for CS:Dex doped with 0, 10, 20, 30, and 40 wt% of NH_4Br, respectively. For the formation of films, the solutions were dried at ambient temperature once it had been cast in various Petri dishes. Solvent-free films were achieved by using a desiccator for the films. All experiments were conducted in controlled condition at 25 °C and relative humidity ~ 50%.

Structural, morphological and impedance characterizations

Fourier transform infrared (FTIR) spectroscopy was conducted alongside 4 cm^{-1} (450–4000 cm^{-1}) resolution by using Spotlight 400 Perkin–Elmer spectrometer. Hitachi SU8220 field emission scanning electron microscopy (FESEM) that has

1 K× magnification was used for analyzing the electrolyte surface. To determine the electrical resistance of the blend films the electrical impedance spectroscopy (EIS) HIOKI 3532-50 LCR HiTESTER was utilized.

Transference number measurement (TNM)

Calculation of ionic (t_{ion}) and electronic (t_{el}) transference number was performed by conducting cell polarization on stainless steel (SS) | maximum conducting SPE | SS with 0.20 V working voltage. Under ambient temperature, there was utilization of V&A Instrument DP3003 digital DC power supply for this evaluation. The following equation can help with calculating t_{ion}:

$$t_{ion} = \frac{I_i - I_{ss}}{I_i} \tag{1}$$

$$t_{el} = 1 - t_{ion} \tag{2}$$

where I_i is the initial current, whereas I_{ss} is the steady state current.

Linear sweep voltammetry (LSV) study

Linear sweep voltammetry (LSV) was used for determining SPE's electrochemical stability. SS | maximum conducting SPE | SS was found to be the LSV evaluation's cell arrangement. Under ambient temperature, Digi-IVY DY2300 potentiostat (10 mV/s scan rate) was used for this evaluation.

EDLC fabrication

Initially, the dry mix procedure was carried out for preparing EDLC electrode. Planetary ball miller was used for dry mixing carbon black (CB) (0.25 g) and activated carbon (AC) (3.25 g). Afterward, they were mixed with the N-methyl pyrrolidone (NMP) (15 mL) and polyvinylidene fluoride (PVdF) (0.5 g) solution. There was an appearance of a thick black solution after stirring the mixture for few hours. Doctor blade was applied for coating this black solution on a current collector (i.e., aluminum foil). The oven was used at a temperature of 60 °C for drying the coated aluminum foil. To further dry these electrodes, there was utilization of a desiccator. For this process, a desiccator consisting of silica gel was used to keep electrodes with 2.01 cm^2 area and thickness of ~ 0.02 cm. AC electrode | maximum conducting SPE | AC electrode was found to show the cell arrangement in the EDLC. A CR2032 coin cell was filled with this cell. First of all, Digi-IVY DY2300 potentiostat (10 mV/s scan rate) was used for conducting the cyclic voltammetry (CV) evaluation on the fabricated EDLC.

Results and discussion

FTIR study

Figure 1 shows the FTIR spectra for pure CS:DEX and all the prepared polymer blend films. A number of researchers have investigated polymer blends using Fourier transform infrared (FTIR) spectroscopy. In the FTIR spectroscopy, bending and stretching vibrations of certain bonds are considered for analyzing FTIR spectra. Therefore, it can provide more information about intermolecular interaction. It has been established that polymer electrolytes comprise both amorphous and crystalline fractions at room temperature. It is known that ion transport principally occurs in the amorphous regions. The reduction in crystalline regions can lead to a relatively high extent of segmental motion which either allows the ions to be hoped from one site to another site or offers a pathway for ions to be moved which result in a high dc conductivity. It is well-established that within a range of 1146–1021 cm^{-1}, the dextran spectra showed its key characteristic bands. Dextran has high chain flexibility close to its glycosidic bonds, which is related to the existence of a peak at the 1021 cm^{-1} [31]. It is exciting to notice that in the blend electrolyte films the OH groups were found in the spectrum of FTIR as broad band at 3351 cm^{-1} [32, 33]. On the contrary, C–H stretching of dextran is responsible for the band at 2906 cm^{-1} as the FTIR spectra of chitosan does not contain this band [34]. The C–H bending was seen at 1400 cm^{-1} where the broad band begins at 1150 cm^{-1}, indicating asymmetrical –C–O–C– stretching of the ring [33]. There are C–O bands signifying the

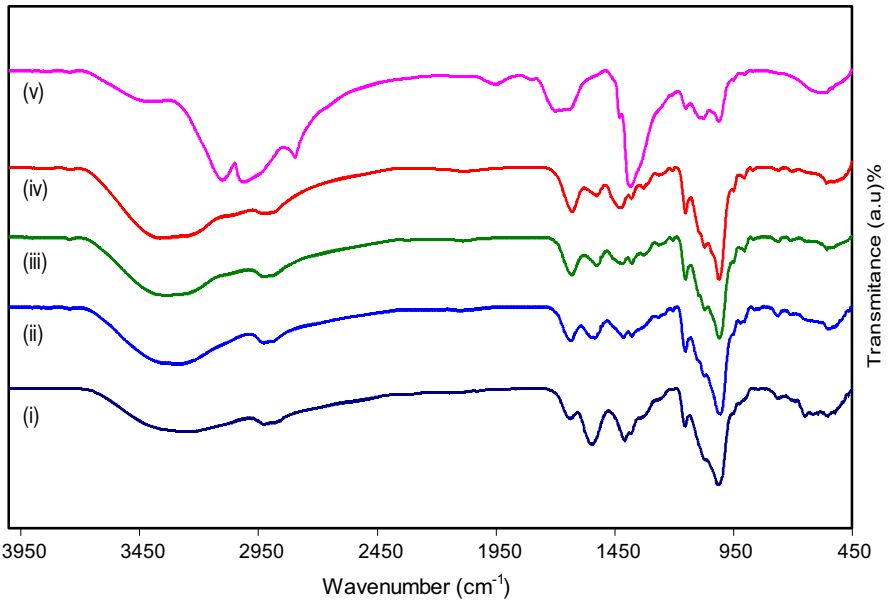

Fig. 1 FTIR spectra of **(i)** CSDex, **(ii)** CSDXN1, **(iii)** CSDXN2, **(iv)** CSDXN3, and **(v)** CSDXN4 in the region from 450 to 4000 cm^{-1}

1067 cm^{-1} small peak and 1009 cm^{-1} sharp one [34]. There was a noticeable peak at 615 cm^{-1} when it comes to dextran C-H configuration [35]. A peak was seen at 1155 cm^{-1} in terms of both stretching vibrations related to the glycosides bridge as well as C–O–C bond. For amine (NH_2) and carboxamide (O=C–NHR) bands, there were two peaks at 1540 cm^{-1} and 1632 cm^{-1}, correspondingly [34]. The dopant salt and CS:Dex have complexation since there was an alteration in the amine (NH_2) and carboxamide (O=C–NHR) bands. Actually, the N–H or O=C–NHR bonds can have reduced vibration intensity as cation salt is attached to oxygen and nitrogen atoms which causes the intensity to shift and lower under the influence of larger molecular weight after the binding of the cations [36]. It is also worth mentioning that the bands had greatly altered intensity because of the combination of NH_4Br salt and CS:Dex. The bands intensity alteration is strongly associated with the change in macromolecular order. The bands in the complexes spectra may be caused by more or less ordered structures [37]. From the FTIR results it is clear that up to 30 wt% of the added salt the bands are broadened and their intensity decreased which is an indicator for the complex formation between the cations of the salt and functional groups of the CS:Dex polymer blend. While at 40 wt% of NH_4Br salt two peaks at 3005 cm^{-1} and 3084 cm^{-1} are emerged, in addition to the intensity increase. According to Hamsan et. al.[6], these two new peaks are attributable to both symmetry vibration and asymmetry vibration of NH_4^+ cation. Thus ion re-association at higher salt concentration is occurs. These results were sorted in Table 1.

Morphological study

The structural variations are related to a variety of mechanisms which can only be understood by considering material morphology. According to pioneer researches, it is possible to get excess of information regarding the alterations by having a look at the morphology of polymers [38, 39]. Based on crystallinity, polymers can be divided into two types: amorphous and crystalline polymers. Amorphous polymers behave like glass or rubber [40]. Our prior research involved studying whether polar polymers

Table 1 The FTIR results of CS:Dex and electrolyte films

Assignments	Wavenumber (cm^{-1})				
	CS:Dex	CSDXN1	CSDXN2	CSDXN3	CSDXN4
C–O band	1009	1001	996	1000	1369
Asymmetrical –C–O–C– stretching	1150	1146	1146	1144	1415
C–H bending	1400	1399	1400	1396	–
NH_2 band	1540	1527	1514	1511	1534
O=C band	1632	1620	1617	1616	1652
C–H stretching	2096	2911	2917	2921	2920
O–H group	3351	3354	3355	3358	3378
Asymmetry vibration (NH_4^+)	–	–	–	–	3084
Symmetry vibration (NH_4^+)	–	–	–	–	3005

accommodated salts with the help of SEM technique [41]. Figure 2a–d presents the FESEM images related to the incorporation of different weight percentage of NH_4Br salt into the CS:Dex systems. The samples surface does not include any protruded particles in Fig. 2a–c and there is smoothness in the surface morphologies of the blend electrolyte films. However, the sample surface in Fig. 2d displays the protrude salts in the form of small white specs. Our previous research was involved the protrusion of particles out of the surface with the addition of 40 wt% salt [42]. Accordingly, it can be seen that there is salt recrystallization as the polymer matrix has a limited capacity to accommodate the additional salts. Moreover, there is a decrease in the value of conductivity at uppermost salt concentration as free ions diminish with the development in recrystallization or ion association [43]. In addition, the ion mobility plays the key role in determining the conductivity of the polymer electrolyte system. The connected network of amorphous regions provides fast ion conducting pathways, which acts upon enhancing the ion mobility and hence the higher ionic conductivity Actually, the added NH_4Br salt and polymer blends had undergone complexation as the samples

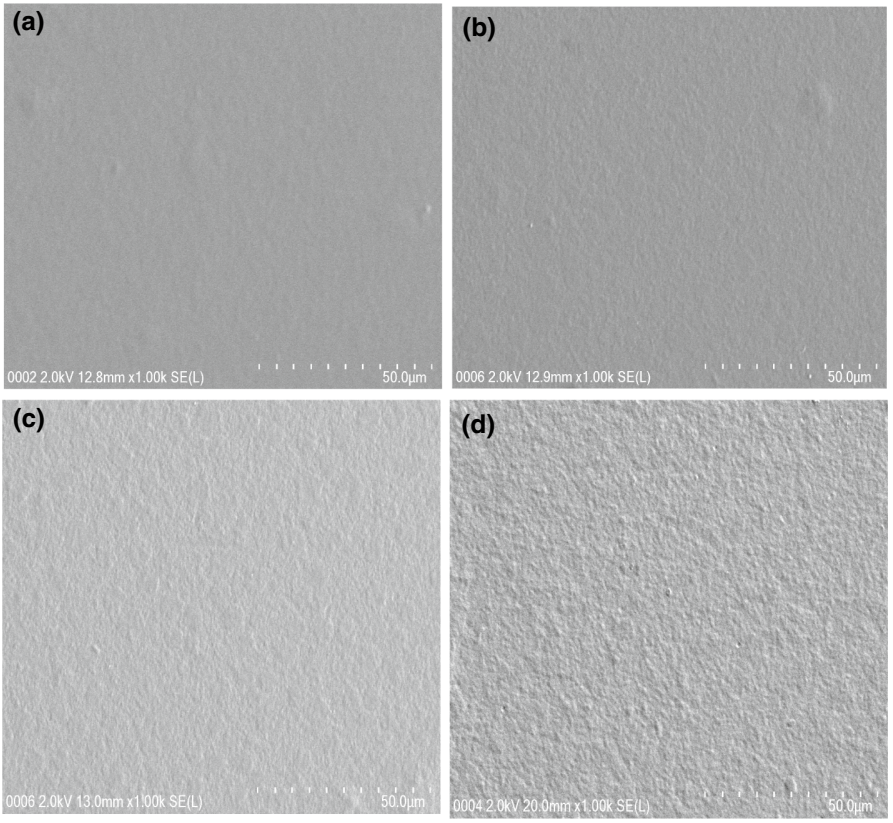

Fig. 2 FESEM images for **a** CSDXN1, **b** CSDXN2, **c** CSDXN3, and **d** CSDXN4 blend films

had smooth surface without phase separation [44], from 10 to 30 wt% of the added NH_4Br salt. These results are well-supported by FTIR outcomes as exhibited in Fig. 1.

Impedance study

It is possible to determine the relaxation frequency and separate the bulk effects (high-frequency semicircular region) from opposite electrodes (low-frequency tail) by using complex impedance spectroscopy (CIS) method. The outcomes of CIS are the real and imaginary parts of impedance (Z' and Z'' respectively) over various frequencies. The DC ionic conductivity of the films has been evaluated with the help of this method [45]. An AC field is applied with different frequencies to the electrochemical sample holder for computing the CIS values [46]. CIS gives the imaginary component of the impedance compared to the real component in the form of a plot which is known as Nyquist plot. In the light of the circuit model, a parallel combination of capacitance and resistance denotes the high-frequency region of the impedance plot. The impedance plot for pure CS:Dextran blend film and electrolyte films at ambient temperature are shown in Fig. 3a–e. Accordingly, Fig. 3a–d has a complex impedance plane where there is a semi-circular Z_{R-C} at high-frequency regions. The electrode/sample interface will have double-layer capacitance considering the low-frequency spike and is represented usually by constant phase element [47]. From the CIS plots it can be seen that the films have bulk relaxation at the high-frequency semicircle with ions migration and accumulation (low-frequency tail) at electrode/electrolyte interface area which causes the declined straight line following the semi-circle [48, 49]. Free charges are developed and accumulated at the electrode surface and SPE interface, which results in the electric double-layer (EDL) capacitances [49]. It is noticeable from Fig. 3a that pure CS:Dextran film possesses large bulk resistance (R_b). Evidently, the R_b value reduces with rising salt concentrations up to 30 wt% as revealed in Fig. 3b–d. From the impedance spectra, it can be seen that a nearly linear curve resides at high salt concentrations (see Fig. 3d, e) that denotes the lower frequency region. This implies that ions play the role of electrolyte current carriers and the conduction mostly results from the ions instead of the electrolyte sample's electrons [50].

In this case, the complex impedance plots belonging to a low-frequency region must display a straight line parallel to the imaginary axis. In other words, the inclination is caused by the blocking double-layer capacitance (electrode polarization) at the electrodes even though the inclination of the straight line should be 90° [51–53].

Figure 3e shows an increase of R_b at 40 wt% NH_4Br salt. This is similar to the findings of FTIR wherein the peaks move to larger wavenumbers at 40 wt% of NH_4Br, showing the ion association and hence conductivity involves fewer ions [6]. It was well-documented that both carrier mobility and density affects the DC conductivity. The equation given below shows the dependence of the degree of conductivity of electrolytes on the number density and the mobility of the ions [30, 34, 42, 49]:

$$\sigma = \sum \eta q \mu \tag{3}$$

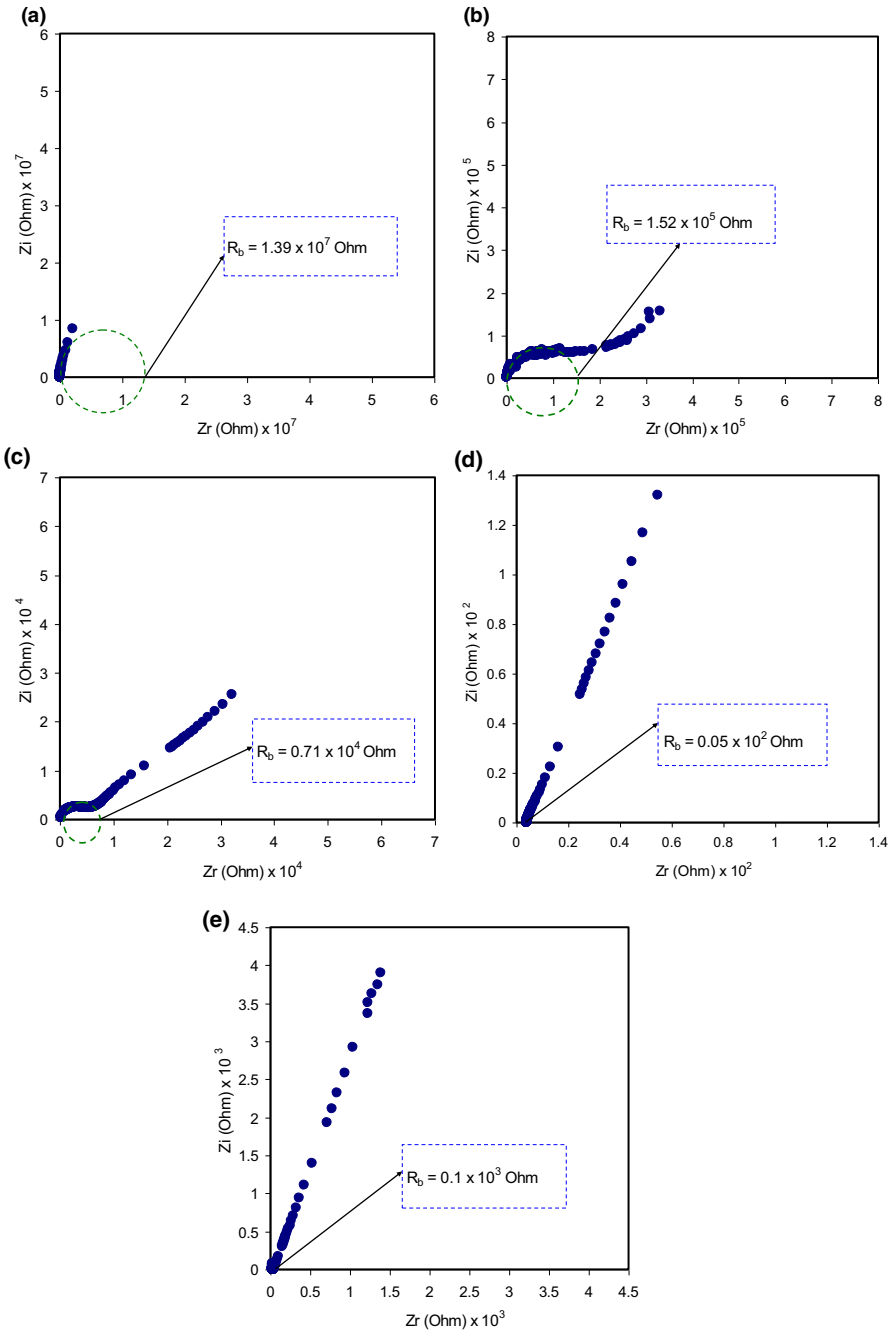

Fig. 3 Impedance plots for **a** CSDex (pure polymers), **b** CSDXN1, **c** CSDXN2, **d** CSDXN3, and **e** CSDXN4 electrolyte films

where η denotes the carrier density, q denotes simple charge and μ represents mobility.

Based on this, the polymer electrolytes ion association can be detected and the FTIR outcomes can be supported with the help of this sensitive method, namely CIS. In addition, CIS can help with determining the phase transition and whether the silver ions of polymer-based electrolytes and composites face reduction, as shown in our earlier reports [41, 54, 55]. The data point evaluation involves the calculation of the R_b value, which is represented by the point where the real axis (Zr) and semicircle intersect. An example of this is that the sample DC conductivity can be determined on the basis of the R_b value and the sample dimensions by using the following equation:

$$\sigma_{dc} = \left(\frac{1}{R_b}\right) \times \left(\frac{t}{A}\right) \tag{4}$$

In this equation, A represents the film surface area and t represents the film thickness. For each sample, the computed DC conductivity can be found in Table 2. In conclusion, blend electrolytes with the highest DC conductivity is a guarantee in the EDLC application.

EDLC study

TNM study

The conduction of ions and electrons results in giving conductivity to the electrolyte. The heart of electrochemical devices is considered to be the ion-conducting electrolyte. It is of significant importance to characterize the electrolytes prior to utilize in the electrochemical devices, for instance batteries and supercapacitors [56]. There has been transference number (TNM) evaluation with working voltage of 0.2 V for determining the major charge carrier. The polarization in the highest conducting CS:Dex:NH_4Br electrolyte is shown in Fig. 4. The cell arrangement for TNM and LSV is shown in Fig. 5. One can notice that when the polarization process initiated, there is a substantial current of 16.5 µA which resulted from the conduction of electrons and ions. The initial current is symbolized by I_i that decreases sharply as time lasts for both of the systems which can be owing to lowering the number of ions in the plasticized polymer electrolytes. At the steady-state, electron migrated along the electrolyte through interface

Table 2 DC ionic conductivity for CS:Dext blend and electrolyte films at room temperature

Sample designation	DC conductivity (S/cm)
CS:Dex	3.84×10^{-10}
CSDXN1	5.43×10^{-8}
CSDXN2	1.16×10^{-6}
CSDXN3	1.64×10^{-3}
CSDXN4	8.28×10^{-5}

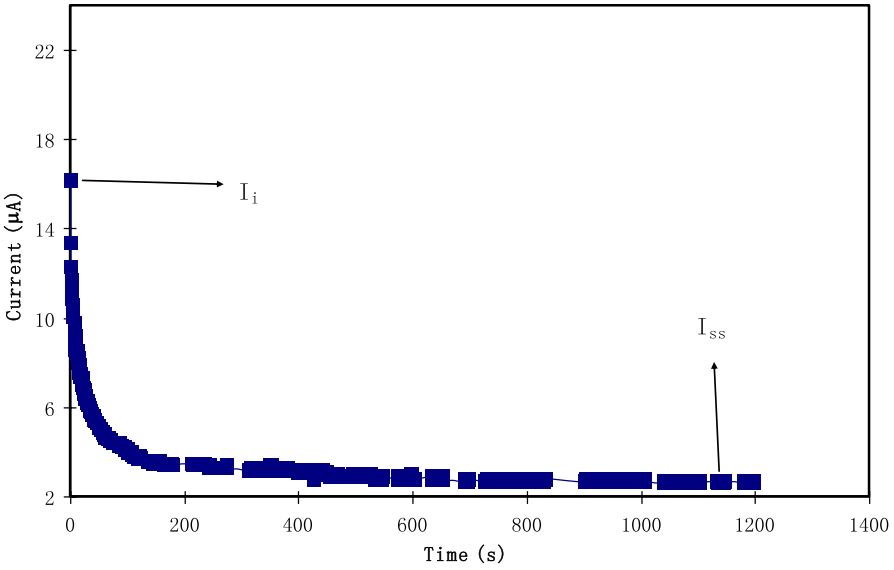

Fig. 4 Polarization current versus time for the highest conducting electrolyte (CSDXN3) film

Fig. 5 Cell arrangement for TNM and LSV

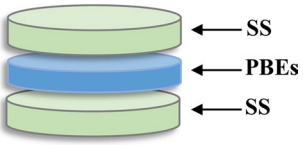

to the electrode that causes polarization [57]. As aforementioned, stainless steel (SS) is the electrode for this evaluation. Since SS only allows electrons to pass through, as it have ion-blocking properties. Due to the fact that SS blocks of ions, there is decay in the current as the time increases until it reaches 2.3 μA and shows a plateau. This steady-state current results in the electrolyte undergoing polarization [58]. With the help of this gathered information, it is possible to use Eqs. (1) and (2) to calculate the value of t_{ion} and t_{el}. The t_{el} value was found to be equal to 0.14 and t_{ion} equal to 0.86. Thus CS:Dex:NH_4Br electrolyte has ions as their primary charge carriers considering that t_{ion} is greater than t_{el}. Cations and anions motions are mainly behind the blend electrolyte film having charge transport [59]. EDLC applications rely on this condition since the surface electrodes face ion accumulation due to the ions. It was found by Vijaya et al. [60], that ammonium salt-based polymer electrolyte has ionic transference numbers in the range from 0.90 to 0.99.

LSV study

Researches related to energy devices require the determination of the electrolyte's potential stability. It is possible to compute the electrolyte's maximum potential

limit in terms of LSV analysis. In Fig. 6, the LSV for the uppermost conducting CS:Dex:NH_4Br electrolyte (with 10 mV/s) has been presented. Lower potential has been seen to provide stability to the current. The electrolyte achieved decomposition potential as there was a drastic increment in current values when the potential reaches 1.54 V. This value is sufficient for the use of the proton-based energy devices. The findings of other researches related to ammonium salt-based polymer electrolyte can be compared with the result of the present work. As per the report of Ng and mohamad [61], CS-based electrolyte exhibited decomposition potential at 1.8 V when the plasticizer was chosen to be ethylene carbonate (EC) and protonic source to be ammonium nitrate (NH_4NO_3). Kadir et al. [62] suggested that there was a maximum potential stability of 1.7 V in CS:Poly(vinyl alcohol) (PVA) blend polymer electrolyte. Accordingly, EDLC can be fabricated using the potential stability of CS:Dex:NH_4Br system.

CV study of EDLC device

Supercapacitor or EDLCs is an important power source for digital communications, memory backups, as well as electric vehicles because it posses long cycle life as well as large power density. Two carbon electrodes (separated by the electrolyte) are usually used in the fabrication of EDLC devices. The non-faradaic reaction and the capacitive behavior of the EDLC can be featured with the help of a suitable tool, namely cyclic voltammetry (CV) [63–65]. CV evaluation can be used for interpreting an EDLC's charge storage mechanism. A range of 0–0.9 V (with 10 mV/s scan rate) was used for conducting the CV analysis of the EDLC device. In Fig. 7, it is possible to see a leaf-shaped CV plot (without redox peaks) for the

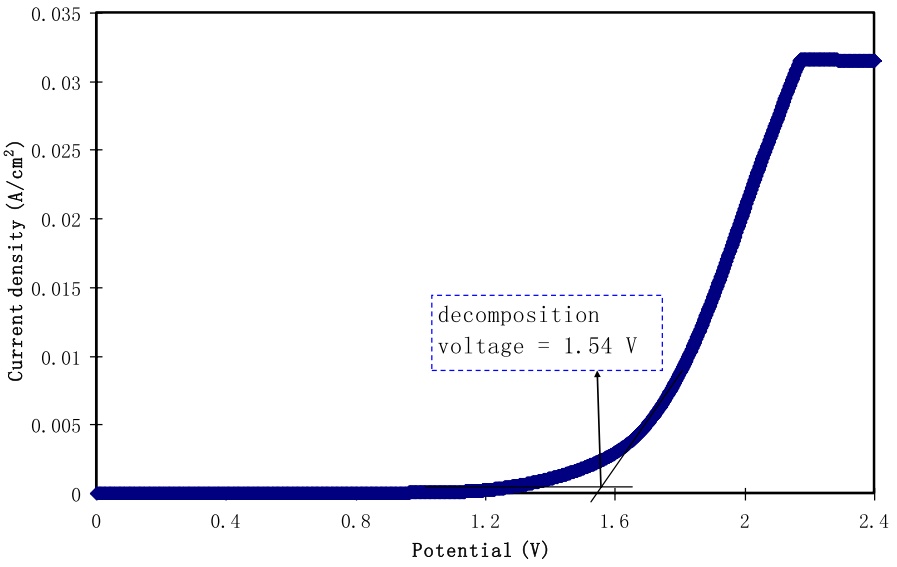

Fig. 6 LSV plot for the highest conducting electrolyte (CSDXN3) film

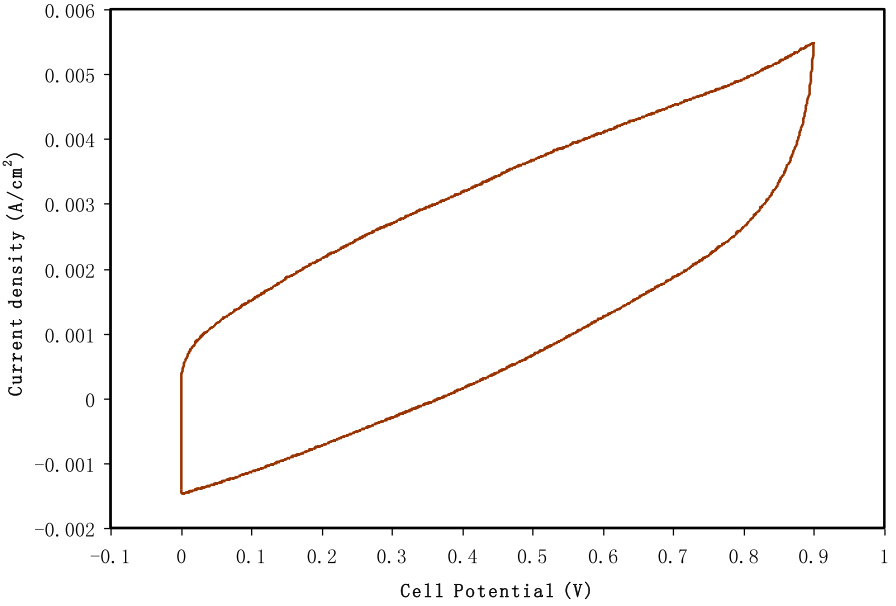

Fig. 7 CV plot for the fabricated EDLC at 10 mV/s

Fig. 8 Schematic illustration of the fabricated EDLC arrangement

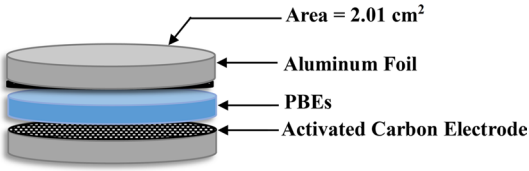

EDLC. As the electrical double-layer experiences ion electrosorption in its electrically charged interface of high surface area carbon electrodes touching an electrolyte, there is accomplishment of energy storage in EDLCs [66]. The arrangement of the fabricated EDLC is shown in Fig. 8. The cell was packed in a CR2032 coin cell-like shape. The electric double-layer capacitive performance is confirmed as the almost mirror image symmetry of current responses to zero [67]. The EDLC did not undergo either oxidation or reduction as no redox peaks were observed in the CV plot. Since of this condition, it can be truly said that the EDLC possesses a capacitive property in which the electrodes face ion accumulation instead of ions undergoing intercalation/deintercation process [68]. Electrical energy can be stored using the following electrochemical objects: batteries as well as electrochemical capacitors. There are Faradaic processes in the first category as the electrode surface either absorbs electrons or sends or receives them from reactants of the solution. On the contrary, there is the absence of faradaic processes in the second case as the surface does not undergo electron transfer. The electrochemical double layer of the interface between the electrolyte and the electrode is charged, which results in charge storage

[69]. Other EDLC researches that have a leaf-shaped CV plot can be compared with the CV plot of this research [70, 71]. As documented by Yusof et al. [71], the shape of the CV plot depends on the scan rate. Internal resistance and electrode porosity are some of the various properties that alter the perfect rectangular shape of the CV [72]. Accordingly, CV evaluation has been used for verifying whether the EDLC shows capacitive behavior. To analyze the obtained results, it is preferable to find the specific capacitance (C_{spe}) of the assembled EDLC from the CV plot via the following equation:

$$C_{spe} = \int_{V_i}^{V_f} \frac{I(V)\mathrm{d}V}{2mv\left(V_f - V_i\right)} \tag{5}$$

where $\int I\,(V)\mathrm{d}V$ is the area of the CV which is determined using the Origin 9.0 software through the integration function. The area of CV plot is found to be 0.00484. The chosen V_i and V_f in the present work are 0 V and 0.9 V, respectively. m and v are the mass of active material used (2.03 mg) and sweep rate (10 $\mathrm{mVs^{-1}}$), respectively. The value of C_{spe} extracted from the CV was 132.5 $\mathrm{Fg^{-1}}$. This value is of great interest from the application and commercialization view points. Table 3 lists various works of carbon-based EDLC and C_{spe} value obtained from CV.

Conclusions

Finally, the preparation of polymer blends based on CS:Dex was done using solution cast technique. There was utilization of FESEM and FTIR routes for studying morphological and structural properties. The added salt and the host polymers had complex development, which can be seen from FTIR bands shift. New peaks in FTIR bands at 40 wt% can be ascribed to ion association. The sample surface exhibited the protrude salts at the highest salt concentration. EIS technique was also used for investigating the samples conductivity. With low salt concentration, it is possible to differentiate between the inclined line at low frequency and the semicircle at high

Table 3 Various carbon-based EDLCs with their respective specific capacitance obtained from CV

Electrolyte	Electrode material	Specific capacitance	Reference
PVA:H_3PO_4	Activated carbon	49.8 (50 mV s^{-1})	[73]
PVA:CH_3COONH_4:BmImI	Activated carbon + Carbon nanotubes	52.78 (10 mV s^{-1})	[74]
Xanthan gum:$LiClO_4$:Glycerol	Activated carbon	74 (5 mV s^{-1})	[75]
Gum:$Li_2B_4O_7$:glycerol	Activated carbon	82 (5 mV s^{-1})	[75]
Chitosan:chitin:LiOAc	Activated carbon cloth	83 (10 mV s^{-1})	[76]
$TEABF_4$:Acrylonitrile	Graphene	99 (20 mV s^{-1})	[77]
KOH	Graphene	100 (20 mV s^{-1})	[77]
CS:Dex:NH_4Br	Activated carbon	132.5	This work

frequency. The conductivity drop at 40 wt% of the added salt is correlated with the results of FESEM and FTIR studies. Moreover, there was ELDC application for the most conducting sample. From the TNM test, it could be seen that the drivers of electrochemical device application, i.e., ion carriers, are almost present in the sample. As per the LSV research, the decomposition of the film took place with above 1.54 V and the sample showed stability with a wide range of potential windows. The fabricated EDLC device was exhibited a capacitive behavior, as it was shown in the CV plot. Since no redox peaks have appeared, it can be said that the EDLC did not undergo either oxidation or reduction. With the help of the CV plot, we have studied more about ions being accumulated at the electrode/electrolyte interface. Large ion accumulation at the electrode/electrolyte interface has been noted from the CV plot. The obtained value of specific capacitance from CV (132.5 Fg^{-1}) is considered promising for commercializing the device.

Acknowledgements The authors gratefully acknowledge the financial support for this study from Ministry of Higher Education and Scientific Research-Kurdish National Research Council (KNRC), KRG/Iraq.

Compliance with ethical standards

Conflict of interest The authors declare no conflicts of interest.

References

1. Orlins S, Guan D (2016) China's toxic informal e-waste recycling: local approaches to a global environmental problem. J Clean Prod 114:71–80
2. Nyuk CM, Isa MIN (2018) Solid biopolymer electrolytes based on carboxymethyl cellulose for use in coin cell proton batteries. J Sustain Sci Manag 2017:42–48
3. Liew CW, Ramesh S, Arof AK (2014) Good prospect of ionic liquid based-poly(vinyl alcohol) polymer electrolytes for supercapacitors with excellent electrical, electrochemical and thermal properties. Int J Hydrog Energy 39:2953–2963
4. Sarwat F, Ahmed N, Aman A, Qader SAU (2013) Optimization of growth conditions for the isolation of dextran producing *Leuconostoc* spp. from indigenous food sources. Pak J Pharm Sci 26(4):793–797
5. Barsbay M, Guner A (2007) Miscibility of dextran and poly(ethylene glycol) in solid state: effect of the solvent choice. Carbohydr Polym 69:214–223
6. Hamsan MH, Shukur MF, Aziz SB, Kadir MFZ (2019) Dextran from leuconostoc mesenteroides doped ammonium salt based green polymer electrolyte. Bull Mater Sci 42:57
7. Misenan MSM, Isa MIN, Khiar ASA (2018) Electrical and structural studies of polymer electrolyte based on chitosan/methyl cellulose blend doped with BMIMTFSI. Mater Res Express 5:5
8. Tyagi A, Joshi MC, Shah A, Thakur VK, Gupta RK (2019) Hydrothermally tailored three-dimensional Ni-V layered double hydroxide nanosheets as high-performance hybrid supercapacitor applications. ACS Omega 4:3257–3267
9. Siwal SS, Zhang Q, Sun C, Thakur VK (2020) Graphitic carbon nitride doped copper–manganese alloy as high–performance electrode material in supercapacitor for energy storage. Nanomaterials 10:2
10. Siwal SS, Zhang Q, Devi N, Thakur VK (2020) Carbon-based polymer nanocomposite for high-performance energy storage applications. Polymers (Basel) 12:1–30
11. Hamsan MH, Shukur MF, Kadir MFZ (2017) The effect of NH_4NO_3 towards the conductivity enhancement and electrical behavior in methyl cellulose-starch blend based ionic conductors. Ionics 23:1137–1154

12. Lee D-Y, An G-H, Ahn H-J (2017) High-surface-area tofu based activated porous carbon for electrical double-layer capacitors. J Ind Eng Chem 52:121–127
13. Guo J, Jiang J, Yang B (2018) Low-voltage electric-double-layer MoS_2 transistor gated via water solution. Solid State Electron 150:8–15
14. Andres B, Dahlstrom C, Blomquist N, Norgen M, Olin H (2018) Cellulose binders for electric double-layer capacitor electrodes: the influence of cellulose quality on electrical properties. Mater Des 141:342–349
15. Yang I, Kim SG, Kwon SH, Lee JH, Kim MS, Jung JC (2016) Pore size-controlled carbon aerogels for EDLC electrodes in organic electrolytes. Curr Appl Phys 16(6):665–672
16. Tran C, Kalra V (2013) Fabrication of porous carbon nanofibers with adjustable pore sizes as electrodes for supercapacitors. J Power Sources 235:289–296
17. Zhao XY, Wu Y, Cao JP, Zhuang QQ, Wan X, He S, Wei XY (2018) Preparation and characterization of activated carbons from oxygen-rich lignite for electric double-layer capacitor. Int J Electrochem Sci 13:2800–2816
18. Xu M, Li D, Yan Y, Guo T, Pang H, Xue H (2017) Porous high specific surface area-activated carbon with co-doping N, S and P for high-performance supercapacitors. RSC Adv 7:43780–43788
19. Iro ZS, Subramani C, Dash SS (2016) A brief review on electrode materials for supercapacitor. Int J Electrochem Sci 11:10628–10643
20. Inagaki M, Konno H, Tanaike O (2010) Carbon materials for electrochemical capacitors. J Power Sources 195(24):7880–7903
21. Zhang D, Zhang X, Chen Y, Yu P, Wang C, Ma Y (2011) Enhanced capacitance and rate capability of graphene/polypyrrole composite as electrode material for supercapacitors. J Power Sources 196(14):5990–5996
22. Pell WG, Conway BE (2004) Peculiarities and requirements of asymmetric capacitor devices based on combination of capacitor and battery-type electrodes. J Power Sources 136(2):334–345
23. Eftekhari A (2019) Surface diffusion and adsorption in supercapacitors. ACS Sustain Chem Eng 7:3692–3701
24. Eftekhari A (2018) The mechanism of ultrafast supercapacitors. J Mater Chem A 6:2866–2876
25. Prajapati GK, Roshan R, Gupta PN (2010) Effect of plasticizer on ionic transport and dielectric properties of PVA–H_3PO_4 proton conducting polymeric electrolytes. J Phys Chem Solids 71:1717–1723
26. Gao H, Lian K (2014) Proton-conducting polymer electrolytes and their applications in solid supercapacitors: a review. R Soc Chem 4:33091–33113
27. Jonson DA (1982) Some thermodynamic aspects of inorganic chemistry, 2nd edn. Cambridge University Press, Cambridge **ISBN 0521242045**
28. Buraidah MH, Arof AK (2011) Characterization of chitosan/PVA blended electrolyte doped with NH_4I. J Non-Cryst Solids 357:3261–3266
29. Kadir MFZ, Hamsan MH (2018) Green electrolytes based on dextran-chitosan blend and the effect of NH_4SCN as proton provider on the electrical response studies. Ionics 24(8):2379–2398
30. Aziz SB, Hamsan MH, Karim WO, Kadir MFZ, Brza MA, Abdullah OGh (2019) High proton conducting polymer blend electrolytes based on chitosan: dextran with constant specific capacitance and energy density. Biomolecules 9(7):267
31. Shukla R, Shukla S, Bivolarski V, Iliev I, Ivanova I, Goyal A (2011) Structural characterization of insoluble dextran produced by *Leuconostoc mesenteroides* NRRL B-1149 in the presence of maltose. Food Technol Biotechnol 49(3):291–296
32. Vettori MHPB, Franchetti SMM, Contiero J (2012) Structural characterization of a new dextran with a low degree of branching produced by *Leuconostoc mesenteroides* FT045B dextransucrase. Carbohyd Polym 88:1440–1444
33. Dumitrascu M, Meltzer V, Sima E, Virgolici M, Albu MG, Ficai A, Moise V, Minea R, Vancea C, Scarisoreanu A, Scarlat F (2011) Characterization of electron beam irradiated collagen-polyvinylpyrrolidone (PVP) and collagen-dextran (DEX) blends. Dig J Nanomater Biostruct 6(4):1793–1803
34. Aziz SB, Abidin ZHZ (2013) Electrical conduction mechanism in solid polymer electrolytes: new concepts to arrhenius equation. J Soft Matter 2013:323868
35. Nikoli GS, Caki M, Mitic Z, Ili B, Premovic P (2009) Attenuated total reflectance-Fourier transform infrared microspectroscopy of copper(II) complexes with reduced dextran derivatives. Russ J Phys Chem A 83:1520–1525

36. Wei D, Sun W, Qian W, Ye Y, Ma X (2009) The synthesis of chitosan-based silver nanoparticles and their antibacterial activity. Carbohyd Res 344(17):2375–2382
37. Mitic ŽO, Cakic M, Nikolic G (2010) Fourier-Transform IR spectroscopic investigations of Cobalt(II)–dextran complexes by using D_2O isotopic exchange. Spectroscopy 24:269–275
38. Hamsan MH, Aziz SB, Shukur MF, Kadir MFZ (2019) Protonic cell performance employing electrolytes based on plasticized methylcellulose–potato starch–NH_4NO_3. Ionics 25:559–572
39. Aziz SB, Abidin ZHZ, Kadir MFZ (2015) Innovative method to avoid the reduction of silver ions to silver nanoparticles in silver ion conducting based polymer electrolytes. Phys Scr 90:035808
40. Hana CC, Shia W, Jin J (2013) Morphology and crystallization of crystalline/amorphous polymer blends. In: Palsule S (ed) Encyclopedia of polymers and composites. Springer, Berlin, pp 1–19
41. Aziz SB, Abdullah RM, Kadir MFZ, Ahmed HM (2019) Non suitability of silver ion conducting polymer electrolytes based on chitosan mediated by barium titanate ($BaTiO_3$) for electrochemical device applications. Electrochim Acta 296:494–507
42. Aziz SB, Abdullah OGh, Rasheed MA, Ahmed HM (2017) Effect of high salt concentration (HSC) on structural, morphological, and electrical characteristics of chitosan based solid polymer electrolytes. Polymers 9(6):187
43. Shukur MF, Kadir MFZ (2015) Hydrogen ion conducting starch–chitosan blend based electrolyte for application in electrochemical devices. Electrochim Acta 158:152–165
44. Aziz SB, Kadir MFZ, Abidin ZHZ (2016) Structural, morphological and electrochemical impedance study of CS:LiTf based solid polymer electrolyte: reformulated Arrhenius equation for ion transport study. Int J Electrochem Sci 11:9228–9244
45. Mahato DK, Dutta A, Sinha TP (2010) Impedance spectroscopy analysis of double perovskite Ho_2NiTiO_6. J Mater Sci 45:6757–6762
46. Aziz SB, Woo TJ, Kadir MFZ, Ahmed HM (2018) A conceptual review on polymer electrolytes and ion transport models. J Science: Adv Mater Devices 3:1–17
47. Pradhan DK, Choudhary RNP, Samantaray BK (2008) Studies of structural, thermal and electrical behavior of polymer nanocomposite electrolytes. eXPRESS Polym Lett 2(9):630–638
48. Qian X, Gu N, Cheng Z, Yang X, Wang E, Dong S (2001) Impedance study of (PEO)10$LiClO_4$–Al_2O_3 composite polymer electrolyte with blocking electrodes. Electrochim Acta 46:1829–1836
49. Aziz SB, Abidin ZHZ (2015) Ion-transport study in nanocomposite solid polymer electrolytes based on chitosan: electrical and dielectric analysis. J Appl Polym Sci 132:41774
50. Yap YL, You AH, Teo LL, Hanapei H (2013) Inorganic filler sizes effect on ionic conductivity in polyethylene oxide (PEO) composite polymer electrolyte. Int J Electrochem Sci 8:2154–2163
51. Jacob MME, Prabaharan SRS, Radhakrishna S (1997) Effect of PEO addition on the electrolytic and thermal properties of PVDF-$LiClO_4$ polymer electrolytes. Solid State Ion 104:267–276
52. Fonseca CP, Cavalcante F Jr, Amaral FA, Souza CAZ, Neves S (2007) Thermal and conduction properties of a PCL-biodegradable gel polymer electrolyte with $LiClO_4$, LiF_3CSO_3, and $LiBF_4$ Salts. Int J Electrochem Sci 2:52–63
53. Aziz SB, Abidin ZHZ, Arof AK (2010) Influence of silver ion reduction on electrical modulus parameters of solid polymer electrolyte based on chitosan-silver triflate electrolyte membrane. eXPRESS Polym Lett 4(5):300–310
54. Aziz SB, Abdullah RM (2018) Crystalline and amorphous phase identification from the tanδ relaxation peaks and impedance plots in polymer blend electrolytes based on [CS:AgNt]x:PEO(x–1) ($10 \leq x \leq 50$). Electrochim Acta 285:30–46
55. Aziz SB, Abidin ZHZ, Arof AK (2010) Effect of silver nanoparticles on the DC conductivity in chitosan–silver triflate polymer electrolyte. Phys B 405(21):4429–4433
56. Marf AS, Abdullah RM, Aziz SB (2020) Structural, morphological, electrical and electrochemical properties of PVA: CS-based proton-conducting polymer blend electrolytes. Membranes 10(4):71
57. Samsudin AS, Kuan ECH, Isa MIN (2011) Investigation of the potential of proton-conducting biopolymer electrolytes based methyl cellulose–glycolic acid. Int J Polym Anal Charact 16:477–485
58. Rani MSA, Ahmad A, Mohamed NS (2017) Influence of nano-sized fumed silica on physicochemical and electrochemical properties of cellulose derivatives-ionic liquid biopolymer electrolytes. Ionics 24:807–814
59. Reddy MJ, Chu PP (2002) Effect of Mg^{2+} on PEO morphology and conductivity. Solid State Ion 149:115
60. Vijaya N, Selvasekarapandian S, Malathi J, Iwai Y, Nithya H, Kawamura J (2013) NMR study on PVP-NH_4Cl based-proton conducting polymer electrolyte. Indian J Appl Res 3:506–510

61. Ng LS, Mohamad AA (2008) Effect of temperature on the performance of proton batteries based on chitosan–NH_4NO_3–EC membrane. J Membr Sci 325:653–657
62. Kadir MFZ, Arof AK (2013) Application of PVA–chitosan blend polymer electrolyte membrane in electrical double layer capacitor. Mater Res Innov 15:217–220
63. Zhu W, Ou X, Lu Z, Chen K, Ling Y, Zhang H (2019) Enhanced performance of hierarchical CuS clusters applying TRGO as conductive carrier for supercapacitors. J Mater Sci Mater Electron 30(6):5760–5770
64. Aziz SB, Brza MA, Mishra K, Hamsan MH, Karim WO, Abdullah RM, Kadir MFZ, Abdulwahid RT (2020) Fabrication of high performance energy storage EDLC device from proton conducting methylcellulose: dextran polymer blend electrolytes. J Mater Res Technol 9:1137–1150
65. Aziz SB, Brza MA, Hamsan MH, Kadir MFZ, Muzakir SK, Abdulwahid RT (2020) Effect of ohmic-drop on electrochemical performance of EDLC fabricated from PVA:dextran:NH_4I based polymer blend electrolytes. J Mater Res Technol. https://doi.org/10.1016/j.jmrt.2020.01.110
66. Jackel N, Rodner M, Schreiber A, Jeongwook J, Zeiger M, Aslan M, Weingarth D, Presser V (2016) Anomalous or regular capacitance? The influence of pore size dispersity on double-layer formation. J Power Sources 326:660–671
67. Fattah NFA, Ng HM, Mahipal YK, Numan A, Ramesh S, Ramesh K (2016) An approach to solid-state electrical double layer capacitors fabricated with graphene oxide-doped. Ionic liquid-based solid copolymer electrolytes. Materials 9:450
68. Pandey GP, Kumar Y, Hashmi SA (2011) Ionic liquid incorporated PEO based polymer electrolyte for electrical double layer capacitors: a comparative study with lithium and magnesium systems. Solid State Ion 190:93–98
69. Costentin C, Porter TR, Saveant JM (2017) How do pseudocapacitors store energy? Theoretical analysis and experimental illustration. ACS Appl Mater Interfaces 9:8649–8658
70. Woo HJ, Liew C, Majid SR, Arof AK (2014) Poly (ε-caprolactone)-based polymer electrolyte for electrical double-layer capacitors. High Perform Polym 26:637–640
71. Yusof YM, Majid NA, Kasmani RM, Illias HA, Kadir MFZ (2014) The effect of plasticization on conductivity and other properties of starch/chitosan blend biopolymer electrolyte incorporated with ammonium iodide. Mol Cryst Liq Cryst 1:73–88
72. Liew CW, Ramesh S (2015) Electrical, structural, thermal and electrochemical properties of corn starch-based biopolymer electrolytes. Carbohydr Polym 124:222–228
73. Hashim MA, Yatim NM, Mahmud NCA, Sazali N, Hamdan D, Yahya MA, Ngah CW, Suhaimi S (2018) Hybrid solid polymer electrolyte from diapers as separator for electrochemical double layer capacitor (EDLC). In AIP conference proceedings, vol 1972, p 020001
74. Liew CW, Ramesh S, Arof AK (2016) Enhanced capacitance of EDLCs (electrical double layer capacitors) based on ionic liquid-added polymer electrolytes. Energy 109:546–556
75. Sudhakar YN, Selvakumar M, Bhat D (2015) Lithium salts doped biodegradable gel polymer electrolytes for supercapacitor application. J Mater Environ Sci 6:1218–1227
76. Stepniak I, Galinski M, Nowacki K, Wysokowski M, Jakubowska P, Jesionowski T (2016) A novel chitosan/sponge chitin origin material as a membrane for supercapacitors—preparation and characterization. RSC Adv 6:4007
77. Stoller MD, Ruoff R (2010) Review of best practice methods for determining an electrode material's performance for ultracapacitors. Energy Environ Sci 3:9

Affiliations

Shujahadeen B. Aziz[1,2] · M. A. Brza[1,3] · H. M. Hamsan[4] · M. F. Z. Kadir[4] · Rebar T. Abdulwahid[1,5]

[1] Advanced Polymeric Materials Research Lab, Department of Physics, College of Science, University of Sulaimani, Qlyasan Street, Sulaimani, Kurdistan Regional Government, Iraq

[2] Department of Civil Engineering, College of Engineering, Komar University of Science and Technology, Sulaimani, Kurdistan Regional Government 46001, Iraq

[3] Department of Manufacturing and Materials Engineering, Faculty of Engineering, International Islamic University of Malaysia, Gombak, Kuala Lumpur, Malaysia

[4] Centre for Foundation Studies in Science, University of Malaya, Kuala Lumpur, Malaysia

[5] Department of Physics, College of Education, University of Sulaimani, Old Campus, Sulaimani, Kurdistan Regional Government, Iraq